



UNIVERSITY OF LEEDS

This is a repository copy of *Co-compartmentalization of Enzymes and Cofactors within Pickering Emulsion Droplets for Continuous Flow Catalysis*.

White Rose Research Online URL for this paper:

<https://eprints.whiterose.ac.uk/191105/>

Version: Supplemental Material

---

**Article:**

Wei, W, Ettelaie, R [orcid.org/0000-0002-6970-4650](https://orcid.org/0000-0002-6970-4650), Zhang, X et al. (4 more authors) (2022) Co-compartmentalization of Enzymes and Cofactors within Pickering Emulsion Droplets for Continuous Flow Catalysis. *Angewandte Chemie International Edition*, 61 (45). e202211912. ISSN 1433-7851

<https://doi.org/10.1002/anie.202211912>

---

© 2022 Wiley-VCH GmbH. This is the peer reviewed version of the following article: Wei, W., Ettelaie, R., Zhang, X., Fan, M., Dong, Y., Li, Z. and Yang, H. (2022), Co-compartmentalization of Enzymes and Cofactors within Pickering Emulsion Droplets for Continuous Flow Catalysis. *Angew. Chem. Int. Ed.*. Accepted Author Manuscript., which has been published in final form at <https://doi.org/10.1002/anie.202211912>. This article may be used for non-commercial purposes in accordance with Wiley Terms and Conditions for Use of Self-Archived Versions. This article may not be enhanced, enriched or otherwise transformed into a derivative work, without express permission from Wiley or by statutory rights under applicable legislation. Copyright notices must not be removed, obscured or modified. The article must be linked to Wiley's version of record on Wiley Online Library and any embedding, framing or otherwise making available the article or pages thereof by third parties from platforms, services and websites other than Wiley Online Library must be prohibited.

Items deposited in White Rose Research Online are protected by copyright, with all rights reserved unless indicated otherwise. They may be downloaded and/or printed for private study, or other acts as permitted by national copyright laws. The publisher or other rights holders may allow further reproduction and re-use of the full text version. This is indicated by the licence information on the White Rose Research Online record for the item.

**Takedown**

If you consider content in White Rose Research Online to be in breach of UK law, please notify us by emailing [eprints@whiterose.ac.uk](mailto:eprints@whiterose.ac.uk) including the URL of the record and the reason for the withdrawal request.



[eprints@whiterose.ac.uk](mailto:eprints@whiterose.ac.uk)  
<https://eprints.whiterose.ac.uk/>

Supporting Information

**Co-compartmentalization of Enzymes and Cofactors within Pickering Emulsion Droplets for Continuous Flow Catalysis.**

Wei Wei, Rammile Ettelaie, Xiaoming Zhang, Min Fan, Yue Dong, Zebiao Li, and Hengquan Yang\*

## Table of Contents

### Experimental procedures

**Table S1.** The total turnover number (TTN) for NADP<sup>+</sup> in literature and in this work.

**Figure S1.** Dodecyl sulfate, sodium salt-polyacrylamide gel electrophoresis (SDS-PAGE) analysis of the AKR solution.

**Figure S2.** Characterizations of the silica emulsifier.

**Figure S3.** Dynamic interfacial tensions in different water/*n*-heptane biphasic systems.

**Figure S4.** Fluorescence microscopy images of Pickering emulsions containing Rhodamine B-labelled AKR or fluorescent NADPH.

**Figure S5.** Concentrations of AKR or NADP<sup>+</sup> before and after the continuous flow for 48 h.

**Figure S6.** Appearance and optical microscopic images of Pickering emulsions (in a fixed-bed reactor) treated with different mobile phases.

**Figure S7.** Conversions with time for the enantioselective reduction of 2-chloro-3',4'-difluoroacetophenone in the Pickering emulsion-based continuous flow systems with different concentrations of 2-octanol.

**Figure S8.** Kinetic profiles for the enantioselective reduction of ethyl 4-chloroacetoacetate in different systems.

**Figure S9.** Conversions with time for the enantioselective reduction of 2-chloro-3',4'-difluoroacetophenone in the Pickering emulsion-based continuous flow systems at different flow rates.

**Figure S10.** Comparison of the specific activity of AKR in batch and continuous flow systems for the enantioselective reduction of 2-chloro-3',4'-difluoroacetophenone.

**Figure S11.** Comparison of the specific activity of AKR in the Pickering emulsion-based continuous flow systems at different flow rates.

**Figure S12.** Conversions with time for the enantioselective reduction of 2-chloro-3',4'-difluoroacetophenone in Pickering emulsion-based continuous flow systems with different concentrations of AKR.

**Figure S13.** Concentrations of AKR in the PBS solution before and after the addition of emulsifier.

**Figure S14.** 2.5D confocal fluorescence microscopy images showing the distribution of Rhodamine B-labelled AKR at the droplet interface at different AKR concentrations.

**Figure S15.** 2.5D confocal fluorescence microscopy images showing the distribution of FITC-labelled solid emulsifier at the droplet interface at different AKR concentrations.

**Figure S16.** The results for the enantioselective reduction of 2-chloro-3',4'-difluoroacetophenone in Pickering emulsion-based continuous flow system at a high concentration of AKR and optical micrographs of the Pickering emulsions.

**Figure S17.** Pickering emulsion-based continuous flow systems with different concentrations of NADP<sup>+</sup>.

**Figure S18.** Optical micrographs of Pickering emulsions with different droplet sizes and the results for the enantioselective reduction of 2-chloro-3',4'-difluoroacetophenone in Pickering emulsion-based continuous flow systems with different droplet sizes.

**Figure S19.** Conversions with time for the enantioselective reduction of 2-chloro-3',4'-difluoroacetophenone in Pickering emulsion-based continuous flow systems with different AKR or NADP<sup>+</sup> concentrations (the amounts of AKR and NADP<sup>+</sup> are fixed and their molar ratio is fixed at about 1:4).

**Figure S20.** Fluorescence intensity of NADPH as a function of time for the case with or without the addition of substrate.

**Figure S21.** Optical micrographs of the Pickering emulsions before and after 300 h of continuous flow reaction.

**Figure S22.** Concentrations of NADP<sup>+</sup> or AKR before and after 300 h of the continuous flow reaction.

**Figure S23.** Scheme illustrations and kinetic plots for batch reactions after standing NADP<sup>+</sup> or AKR at 30 °C for 300 h.

**Figure S24.** Scheme illustrations and kinetic plots of different experiments reveal the reason for enzyme deactivation.

**Figure S25.** SDS-PAGE analysis of the TA solution.

**Figure S26.** Fluorescence microscopy images of Pickering emulsions containing Rhodamine B-labelled TA or fluorescent PLP.

**Figure S27.** Comparison of the catalytic efficiency of TA in batch and continuous flow systems for the enantioselective transamination of 4'-nitroacetophenone.

### References

### Mass spectrometry data for various compounds encountered in this study

## Experimental procedures

### Chemicals and reagents

Toluene (AR), *n*-heptane (AR), sodium dihydrogen phosphate ( $\text{NaH}_2\text{PO}_4$ ), dibasic sodium phosphate ( $\text{Na}_2\text{HPO}_4$ ), acetic anhydride (99%) Rhodamine B (99%), Coomassie Brilliant Blue G-250 (CBB) and bovine serum albumin (BSA) were procured from Sinopharm Chemical Reagent Co., LTD, (China). (Octyl)trimethoxysilane (98%), tetraethyl orthosilicate (TEOS, AR), 4-dimethylaminopyridine (98), *n*-hexanol (AR), 2-octanol (AR), 2,3,4'-trichloroacetophenone (98%), 2-chloro-2',4'-difluoroacetophenone (98%), methyl benzoylformate (97%), 2,2,2-trifluoroacetophenone (97%), ethyl 4-chloroacetoacetate (95%), 2-chloro-3',4'-difluoroacetophenone (98%), 4'-nitroacetophenone (98%), 3'-nitroacetophenone (98%) 1-phenylethylamine (98%), methyl DL-mandelate (99%), ethyl-4-chloro-3-hydroxybutyrate (98%), 2,2,2-trifluoro-1-phenylethanol (98%), 1-(4-nitrophenyl)ethanamine (98%), 1-(3-nitrophenyl)ethanamine (98%),  $\beta$ -Nicotinamide adenine dinucleotide phosphate sodium salt hydrate ( $\text{NADP}^+$ , 97%), pyridoxal 5-phosphate monohydrate (PLP, 98%),  $\text{NaBH}_4$  and triethylamine (99%) were purchased from Aladdin (China). FITC-dextran (CAS No. 60842-46-8) was obtained from Santa Cruz Biotechnology. Cyclohexane (AR) and Triton X-10 (TX-10, 98%) were obtained from Guangzhou Reagent Company (China). The AKR solution and TA solution were provided by Nantong Chanyoo Pharmatech Co., Ltd. Water used in this study was de-ionized water.

### Characterization

Transmission electron microscopy (TEM) images were obtained using a JEOL-JEM-2000EX instrument. Samples for TEM observation were prepared by dispersing the corresponding powder in ethanol using ultrasound and then allowing a drop of the suspension to evaporate on a copper grid covered with a holey carbon film. Nitrogen-sorption measurements were performed at  $-196\text{ }^\circ\text{C}$  on a Micromeritics ASAP 2020 analyzer. Before measurements, samples were degassed at  $120\text{ }^\circ\text{C}$  under vacuum for 6 h. The surface area was calculated from the adsorption branch in the relative pressure range of 0.05–0.15 using the Brunauer-Emmett-Teller (BET) method. The dynamic interfacial tension was measured using a DCAT21 tensiometer (Dataphysics Company, Germany). The contact angles were measured with a Krüss DSA100 instrument. For measurements, the powder samples were compressed into a disk of thickness approximately 1 mm (ca. 2 MPa). A drop of water (1  $\mu\text{L}$ ) was injected on top of the sample disk. The appearance of water drop was recorded at ca. 0.1 second with a digital camera. Thermogravimetric analysis (TG) measurement was performed on TA Q-600 instrument. UV-Vis determination was conducted on a TU-1900 spectrometer (China). The contact angle was determined by using a photo goniometric method. Emulsion droplets were observed using an optical microscope (XSP-8CA, Shanghai, China) equipped with 10  $\times$  magnification lens. Gas chromatography (GC) analysis was carried out on an Agilent 7890 analyzer (HP-CHIRAL-20B) with a flame ionization detector. The identification of products by mass spectrometry (MS) was performed on a GC-MS instrument (7890A-5977A, HP-5, Agilent). Confocal laser scanning microscopy images were obtained by a Carl Zeiss LSM880 instrument (Germany). The concentration of FITC-dextran in water was  $5 \times 10^{-6}\text{ M}$  and the excitation wavelength is 488 nm (green). The concentration of Rhodamine B in water was  $2 \times 10^{-3}\text{ M}$  and the excitation wavelength is 554 nm (red). The enantioselectivities of products were determined by comparing their corresponding racemic compound by GC analysis; the configurations of chiral products were confirmed with a polarimeter.

### Synthesis of partially hydrophobic silica emulsifier.

Silica nanospheres were prepared according to our previous method.<sup>[1]</sup> 1.5 g of synthesized silica nanospheres (dried at  $120\text{ }^\circ\text{C}$  for 4 h) were dispersed into toluene (8 mL), followed by adding a mixture of 4.5 mmol  $(\text{MeO})_3\text{SiC}_8\text{H}_{17}$  and 4.5 mmol  $(\text{C}_2\text{H}_5)_3\text{N}$ . After reflux for 4 h, the resultant solid product was isolated through centrifugation, washed four times with toluene and dried under vacuum, yielding methyl-modified silica particles as emulsifiers.

### Preparation of Rhodamine B-labelled enzyme.

2 mL of aqueous solution of AKR and 200  $\mu\text{L}$  of aqueous solution of Rhodamine B ( $2 \times 10^{-3}\text{ M}$ ) were added into a PBS solution (2 mL, phosphate buffer: 0.1 M  $\text{Na}_2\text{HPO}_4$ , 0.1 M  $\text{NaH}_2\text{PO}_4$ , pH 7.4). The mixture was stirred at room temperature in the dark for 12 h. The resultant solid Rhodamine B-labelled AKR was isolated through centrifugation, and washed with PBS four times, eventually giving Rhodamine B-labelled AKR.

### Batch reactions

Biphasic reactions in batch were conducted in a 20 mL glass vial. Generally, 3.6 mL of PBS solution containing  $\text{NADP}^+$  (80  $\mu\text{M}$ ) and AKR (0.58  $\text{mg mL}^{-1}$  of protein, 0.92  $\text{U mg}^{-1}$ ) was added into 1.8 mL of *n*-heptane containing substrate (0.1 M) and 2-octanol (0.24 M). The reaction mixture was stirred with a magnetic stir bar (10 mm in length, 600 rpm) at  $30\text{ }^\circ\text{C}$ . An aliquot of oil phase was taken at intervals for monitoring conversions by GC. For Pickering emulsion reactions in batch, the procedures are similar to this procedure, except for the addition of 0.15 g of emulsifier for emulsification (stirring at 5000 rpm for 1 min).

### Determination of the enzyme specific activity

The enantioselective reduction was carried out in 1.0 mL PBS containing 0.10 mmol 2-chloro-3',4'-difluoroacetophenone, 0.24 mmol 2-

octanol, 80  $\mu\text{M}$  NADP<sup>+</sup> and a certain amount of AKR. After reaction at 30 °C for 5 min, the reaction was stopped by adding 50  $\mu\text{L}$  of H<sub>2</sub>SO<sub>4</sub>. The sample was assayed by GC. One unit (U) of enzyme activity was defined as the amount of enzyme generating 1  $\mu\text{mol}$  product per minute under the standard assay conditions. The specific activity of AKR was calculated as 0.92 U mg<sup>-1</sup>.

#### **AKR-catalyzed enantioselective reduction reactions.**

In a typical AKR-catalyzed enantioselective reduction of ketone in Pickering emulsion-based continuous flow systems, a mixture of 3.6 mL of enzyme solution (0.58 mg mL<sup>-1</sup> AKR, 80  $\mu\text{M}$  NADP<sup>+</sup>), 1.8 mL of *n*-heptane and 0.15 g of emulsifier was stirred at 5000 rpm for 1 min, resulting in a Pickering emulsion. This Pickering emulsion was then poured into a glass column reactor (1.34 cm in inner diameter) with a sand filter (4.5-9  $\mu\text{m}$  in pore diameter) and valve at the bottom. The solution of the substrate (0.1 M) and 2-octanol (0.24 M) in *n*-heptane at a given velocity was continuously pumped into the column and passed through the column reactor whose temperature was maintained at 30 °C. The outflow from the column bottom was sampled for GC analysis at intervals.

#### **Enantioselective reduction of 2-chloro-3',4'-difluoroacetophenone with different concentrations of AKR**

The procedures are the same as those applied in the **AKR-catalyzed enantioselective reduction reaction** except that the concentration of AKR was varied from 0.145 to 4.64 mg mL<sup>-1</sup>.

#### **Enantioselective reduction of 2-chloro-3',4'-difluoroacetophenone with different concentrations of cofactor**

The procedures are the same as those applied in the **AKR-catalyzed enantioselective reduction reaction** except that the concentration of NADP<sup>+</sup> was varied from 0.011 to 80  $\mu\text{M}$ .

#### **Enantioselective reduction of 2-chloro-3',4'-difluoroacetophenone with different concentrations of AKR and cofactor**

The procedures are the same as those applied in the **AKR-catalyzed enantioselective reduction reaction** except that the amount of water was tuned from 0.45 to 3.6 mL and the emulsifier amount was varied from 0.019 to 0.15 g.

#### **Enantioselective reduction of 2-chloro-3',4'-difluoroacetophenone with different droplet sizes**

The procedures are the same as those applied in the **AKR-catalyzed enantioselective reduction reaction** except that the droplet size was varied from 23 to 77  $\mu\text{m}$ . Emulsification with ultrasonic cell crusher (200 w for 1 min) led to Pickering emulsion droplets with an average size of 23  $\mu\text{m}$ ; emulsification with stirring (5000 rpm for 1 min) resulted in Pickering emulsion droplets with an average size of 41  $\mu\text{m}$ ; emulsification with stirring vigorously shaking (800 rpm for 3 min) generated Pickering emulsion droplets with an average size of 77  $\mu\text{m}$ .

#### **TA-catalyzed enantioselective transamination reactions.**

In a typical TA-catalyzed enantioselective transamination of ketone in Pickering emulsion-based continuous flow systems, a mixture of 6.0 mL of enzyme solution (2.16 mg mL<sup>-1</sup> TA, 0.75 mM PLP), 3.0 mL of toluene and 0.18 g of emulsifier was stirred at 5000 rpm for 1 min, resulting in a Pickering emulsion. This Pickering emulsion was then poured into a glass column reactor (1.34 cm in inner diameter) with a sand filter (4.5-9  $\mu\text{m}$  in pore diameter) and valve at the bottom. The solution of substrate (0.05 M) and 1-phenylethylamine (0.2 M) in toluene at a given velocity was continuously pumped into the column and passed through the column reactor whose temperature was maintained at 45 °C. The outflow from the column bottom was sampled for GC analysis at intervals.

#### **Retention fraction of AKR and NADP<sup>+</sup> determination**

First, a Pickering emulsion containing AKR and NADP<sup>+</sup> was prepared according to the method applied in the **AKR-catalyzed enantioselective reduction reaction**. This emulsion was then gently poured into a glass column reactor (1.34 cm in inner diameter) with a sand filter (4.5-9  $\mu\text{m}$  in pore diameter) and valve at the bottom. *n*-Heptane as mobile phase was continuously pumped into the column and passed through the column reactor whose flow rate was maintained at 5 mL h<sup>-1</sup>. After flowing for 48 h, the Pickering emulsion collected from the column was demulsified through centrifugation. The concentrations of AKR and NADP<sup>+</sup> in the obtained aqueous solution were determined through UV-Vis spectrophotometry. To eliminate the possible effect of the presence of silica (AKR and NADP<sup>+</sup> were adsorbed on silica particles), the fresh Pickering emulsion was subjected to the same treatment for determination. The retention fraction is the ratio of the amount of AKR or NADP<sup>+</sup> after flow to its amount before flow.

#### **Determination of protein content (Bradford method<sup>[2]</sup>)**

The Bradford reagent was prepared according to the following protocol. 100 mg of Coomassie brilliant blue G-250 (CBB) and 100 mL of 85% phosphoric acid were dissolved in 50 mL 95% ethanol. This solution was then diluted to one liter with distilled water.

**Protein assay:** Briefly, 1 mL of the sample was mixed with 4 mL of Bradford reagent in a cuvette. The resultant mixture was incubated for 10 min at room temperature for UV-Vis determination (595 nm). Bovine albumin serum (BAS) was processed by the same method

and used as a standard. Absorbance values from analyzed samples were interpolated in the standard curve equation to obtain the protein concentration. All samples and standards were processed in triplicates.

**References**

(1) D. Y. Kong, C. M. Zhang, Z. H. Xu, G. G. Li, Z. Y. Hou, J. Lin, *J. Colloid Interface Sci.* **2010**, 352, 278-284.  
 (2) M. M. Bradford, *Anal. Biochem.* **1976**, 72, 248-254.

**Theoretical calculation**

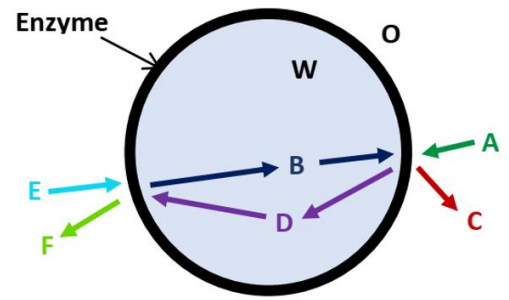
The reactions discussed in the main text in the paper can more generally be modelled in the following manner. We consider the situation depicted by the figure below, where two reactions



and



occur at an interfacial region (indicated by the dark black line) around the surface of droplets. A suitable enzyme, catalyzing the reactions, is adsorbed at this interfacial region. The components A, C, E and F are all oil-soluble, but highly insoluble in water, whereas B and D are water-soluble and therefore only confined to the interior of the water droplets. The reaction constants for the forward reactions, per unit surface area, are denoted by  $k_1$  and  $k_3$ , respectively<sup>1</sup>. For the type of reaction we are considering here, the backward reactions are sufficiently slow and can safely be ignored<sup>2</sup>. As there are no reactions taking place in bulk water or oil, the concentration profiles in both these phases are governed by the diffusion equation



(1)

Where  $X = A, B, C, D, E$  or  $F$  represents the concentration of each component, and  $d_f^i$  is the diffusion coefficient with  $i = o$  or  $w$ , depending on whether the component resides in water (as for B and D) or in the oil phase (as for A, C, E and F)<sup>3</sup>. Under steady-state conditions, all the time dependencies of the concentration profiles vanish. Therefore, equation (1) reduces to  $\nabla^2 X = 0$ . When this is expressed in the spherical polar coordinates, and the advantage of the spherical symmetry of the problem taken, the equation further reduced to

$$\frac{1}{r} \frac{\partial^2}{\partial r^2} (rX) = 0 \tag{2}$$

The solution to (2) has the well-known form

$$X(r) = b_1^x + \frac{b_2^x}{r} \tag{3}$$

where  $b_1^x$  and  $b_2^x$  are constants of integration to be determined by the appropriate boundary conditions, as discussed later below. Now, for B and D inside the droplet, the concentrations need to remain finite even at  $r = 0$ . For both of these then  $b_2 = 0$ . Thus, we arrive at the important result that at steady-state there are no diffusion fluxes within the droplets. Under such conditions, the concentrations of B and D are uniform inside the emulsion drops.

With no diffusion in or away from the surface, the above results also imply that the rates of conversion of B to D and that of D back to B occurring at the interface, must equal each other when the steady-state is achieved. That is to say we have

$$k_1 A_R B = k_3 E_R D \tag{4}$$

where  $A_R$  and  $E_R$  denote the concentrations of A and E reactants on the surface of droplets. Furthermore, the conservation of the total amount of (D+B) means that

$$B + D = B^{in} \quad . \quad (5)$$

Here  $B^{in}$  is the initial specified concentration of B in the droplet at time  $t=0$ , when no component D is present in the system. Combining (4) and (5) we arrive at

$$B = \left( 1 + \frac{k_1 A_R}{k_3 E_R} \right)^{-1} B^{in} \quad (6)$$

and

$$D = \left( 1 + \frac{k_3 E_R}{k_1 A_R} \right)^{-1} B^{in} \quad . \quad (7)$$

Next, let us calculate  $A_R$  and  $E_R$ . For A and E the bulk concentration of reactants in the oil phase is given. These will be denoted as  $A_\infty$  and  $E_\infty$ . From equation (3) we then have constant  $b_1^a = A_\infty$  for the component A and  $b_1^e = E_\infty$  for E. The other constant  $b_2$  is obtained by considering the rate at which A and E are being consumed at the interface and by equating this with the diffusive flux of these incoming molecules arriving at the surface. That is to say

$$d_f^o \frac{\partial A}{\partial r} \Big|_{r=R} = \frac{-d_f^o b_2^a}{R^2} = k_1 B A_R$$

and

$$d_f^o \frac{\partial E}{\partial r} \Big|_{r=R} = \frac{-d_f^o b_2^e}{R^2} = k_3 D E_R$$

which in turn, when combined with equation (3), gives the radial dependent concentrations of A and E as

$$A(r) = \frac{-k_1 B A_R R^2}{d_f^o r} + A_\infty \quad (8)$$

and

$$E(r) = \frac{-k_3 D E_R R^2}{d_f^o r} + E_\infty \quad . \quad (9)$$

Equations (8) at  $r=R$  should evaluate to  $A_R$ . Therefore,

$$A_R = \frac{-k_1 B A_R R}{d_f^o} + A_\infty$$

Leading to the following relation between  $A_R$  and  $A_\infty$

$$A_R = \left( 1 + \frac{k_1 B R}{d_f^o} \right)^{-1} A_\infty \quad . \quad (10)$$

A similar result can be obtained for  $E_R$  by considering equation (9) at  $r = R$

$$E_R = \left( 1 + \frac{k_3 D R}{d_f^o} \right)^{-1} E_\infty \quad . \quad (11)$$

Substituting (5), (10) and (11) back in (6), we arrive at

$$B = \frac{k_3 (d_f^o + k_1 R B) E_\infty B^{in}}{k_3 (d_f^o + k_1 R B) E_\infty + k_1 (d_f^o + k_3 R (B^{in} - B)) A_\infty} \quad (12)$$

which after rearranging yields the following quadratic equation for B

$$Z B^2 + Y B + W = 0 \quad . \quad (13)$$

Here for conciseness we have defined

$$Z = k_1 k_3 R (E_\infty - A_\infty)$$

$$Y = d_f^o (k_1 A_\infty + k_3 E_\infty) - k_1 k_3 R B^{in} (E_\infty - A_\infty)$$

$$W = -k_3 d_f^o E_\infty B^{in}$$

Equation (13) has the following two solutions

$$B = \frac{-Y \pm \sqrt{Y^2 - 4ZW}}{2Z} \quad , \quad (14)$$

but of these only the physically meaningful one is of interest to us. With B now determined, it is an easy matter to calculate the values of D, and hence  $A_R$  and  $E_R$  viz. equations (5), (10) and (11). In particular, it is also possible then to obtain the rate of generation of the product C per unit surface, i.e.  $k_1 B A_R$ . Similarly, the specificity with respect to component B (i.e. the rate of production of C per mole of  $B^{in}$ ), is calculated as follows:

$$\frac{4\pi R^2 k_1 B A_R}{\left( \frac{4}{3} \pi R^3 B^{in} \right)} = \frac{3k_1 B A_R}{R B^{in}} = \frac{3k_1 A_R}{R \left( 1 + \frac{k_1 A_R}{k_3 E_R} \right)} = \frac{3k_1 k_3 A_R E_R}{R (k_3 E_R + k_1 A_R)} \quad (15)$$

The exact rate of conversion and the specificity behavior for the system can be calculated using the model above. However, this requires experimental values of various parameters including  $k_1$  and  $k_3$ . Unfortunately, these are not always easy to measure. However, it is still

possible to predict certain trends for the conversion and the associated specificities under certain conditions. Two such cases arise when  $A_\infty \gg E_\infty$  or alternatively if  $|A_\infty - E_\infty| \ll A_\infty$ . In both cases  $4ZW \ll Y^2$  and one can approximate (14) as

$$B = \frac{-Y \pm \sqrt{Y^2 - 4ZW}}{2Z} = \frac{Y}{2Z} \left( \sqrt{1 - \frac{4ZW}{Y^2}} - 1 \right) \approx \frac{-W}{Y} \quad . \quad (16a)$$

For the second of these cases, this further simplifies to

$$B \approx \frac{-W}{Y} \approx \frac{k_3 E_\infty}{(k_3 E_\infty + k_1 A_\infty)} B^{in} \quad . \quad (16b)$$

Substituting the above equation in (10) gives the value of  $A_R$ :

$$A_R = \left( 1 + \frac{R}{d_f^o} \frac{k_1 k_3 E_\infty}{(k_3 E_\infty + k_1 A_\infty)} B^{in} \right)^{-1} A_\infty \quad . \quad (17a)$$

Similarly, in combination with (5) and (11), for  $E_R$  we obtain:

$$E_R = \left( 1 + \frac{R}{d_f^o} \frac{k_1 k_3 A_\infty}{(k_3 E_\infty + k_1 A_\infty)} B^{in} \right)^{-1} E_\infty \quad . \quad (17b)$$

Thus, the rate of conversion per droplet is given as

$$\begin{aligned} 4\pi R^2 k_1 B A_R &= \left( 4\pi R^2 A_\infty B^{in} \right) \frac{k_1 k_3 E_\infty}{(k_3 E_\infty + k_1 A_\infty)} \left( 1 + \frac{R}{d_f^o} \frac{k_1 k_3 E_\infty}{(k_3 E_\infty + k_1 A_\infty)} B^{in} \right)^{-1} \\ &= \left( \frac{\Theta}{1 + \Omega \Theta} \right) \left( 4\pi R^2 k_1 A_\infty B^{in} \right) \end{aligned} \quad (18)$$

where we have defined the following two important parameters

$$\Omega = \frac{k_1 R B^{in}}{d_f^o} \quad (19)$$

and

$$\Theta = \frac{k_3 E_\infty}{(k_3 E_\infty + k_1 A_\infty)} \quad (20)$$

The dimensionless quantity  $\Omega$  is an indicator of the time scale for diffusion relative to the time scale for the reactions. When it is much larger than  $1/\theta$ , it indicates that the slow diffusion of the reactants from the oil side is the significant factor in limiting the rate of conversion. On the other hand, when  $\Omega$  is much smaller than  $1/\theta$ , the low concentration of B in the droplets, and hence the subsequent slow rate of

reactions on the interface, become the rate-limiting step that hinders the rapid conversion of A to the desired compound C. As for the parameter  $\theta$ , this roughly indicates the proportion of initial B (i.e.  $B^{in}$ ) in the droplets that has remained as B, once steady state is achieved<sup>4</sup>. The remainder of course, is the steady-state value for the concentration of D.

Using equation (18), the rate of conversion per initial mole of B under same steady-state conditions is given as

$$\left( \frac{\Theta}{1 + \Omega\Theta} \right) \frac{(4\pi R^2 k_1 A_\infty B^{in})}{\frac{4}{3}\pi R^3 B^{in}} = \left( \frac{\Theta}{1 + \Omega\Theta} \right) \frac{3k_1 A_\infty}{R} \quad (21)$$

At sufficiently low initial concentration  $B^{in}$ , where  $\Omega\theta \ll 1$ , we predict that the specificity approaches  $3\theta k_1 A_\infty / R$ . This, as can be noted, is completely independent of  $B^{in}$  (but interestingly also of  $d_f^0$ ). The expression also shows that, with all else being the same, the specificity improves as the droplet size becomes smaller in this regime. However, at larger concentrations, where  $\Omega\theta \gg 1$ , equation (21) leads to

$$\frac{3k_1 A_\infty}{\Omega R} = \frac{3d_f^0 A_\infty}{R^2 B^{in}} \quad (22)$$

It is clear that in such circumstances the conversion rate per mole of B decreases as  $1/B^{in}$ . It is interesting that the specificity in this regime is now independent of the reaction rate constants,  $k_1$  and  $k_3$ , but varies only with the diffusion coefficient of A and E in the oil phase. This of course may be expected. In this regime the reactions progress fast enough (as relative to diffusion of A and E to the surface) for them not be rate limiting. It is the diffusion process that now governs how fast the conversion can proceed. In this same regime, the improvement in the specificity with smaller size of droplets is found to be even more pronounced, varying as  $1/R^2$ , as opposed to  $1/R$  in low  $B^{in}$  systems<sup>5</sup>.

The above conclusions were arrived at on the basis of our analysis for the case where  $|A_\infty - E_\infty| \ll A_\infty$ . We have also performed similar calculations for systems where  $A_\infty \gg E_\infty$ , where again suitable simplifying approximations are possible. The conclusions are very similar. This tends to suggest that parameter  $\Omega$  remains a good indicator of whether the conversion is governed by diffusion or by reactions on the surface of droplets, even in circumstances where the above conditions may be relaxed. In particular, we expect quite generally that the specificity approaches a constant value at low  $B^{in}$ , whereas it varies as  $1/B^{in}$  at higher initial concentrations of B. These trends do seem to agree well and are borne out qualitatively by our experimental results.

#### NOTE

1. Note that the SI units of  $k_1$  and  $k_3$ , as defined here, are in  $m^4/mol/s$ , so as to make the equation rates as per unit surface area, i.e. mole/s/m<sup>2</sup>.
2. This is because C and F diffuse relatively quickly away from the surface back into the oil phase (where their bulk concentrations remain relatively low close to zero). Therefore, concentration of these on the surface is always low. As for conversion of B to D and vice versa, this is largely dominated by the forward reactions, therefore allowing the much slower backward reactions to be ignored.
3. We take the diffusion coefficient of all components in the oil phase to be the same and that of B and D in water also equal to each other. This reasonable simplification does not drastically alter the conclusions.
4. This statement becomes increasingly more accurate as the rate of reactions on the surface become slower. This is because for very slow reactions, the concentrations of A and E on the surface approach their bulk values,  $A_\infty$  and  $E_\infty$ , respectively. With  $A_R \approx A_\infty$  and  $E_R \approx E_\infty$ , it is easy to see from equation (6) that  $B = \theta B^{in}$ .
5. This is provided that there is enough AKR remaining in the system to fully cover and maintain the same full saturation coverage on the surface of the droplets, as  $R$  is reduced. With the same saturation coverage of AKR, the values of the reaction rate constants  $k_1$  and  $k_3$  are then maintained at the same values for droplets of all sizes. If this was not the case, then the interfacial coverage of AKR will alter with changing  $R$  and the effect on  $k_1$  and  $k_3$  needs to be accounted for. For example, if the coverage of the surface by AKR at some droplet radius  $R_0$  is  $\Gamma_0$ , such that almost all of AKR is already at the interface, then at a smaller droplet size of  $R$  the coverage will only be  $\Gamma(R) = (R/R_0)\Gamma_0$ . This is to say that the value of  $k_1$  and  $k_3$  are now expected to increase linearly with  $R$ , and as such will be smaller in a system with finer sized droplets.

**Table S1:** Total turnover numbers (TTN) for NADP<sup>+</sup> in literature and in this work.

Systems	substrates	Method	Conversion	TTN	Reference
Enzymes and cofactors were co-immobilized onto polyethyleneimine-modified agarose microbeads	2,2,2-trifluoro-1-phenyl-ethanone	Flow system	80%	85	Angew. Chem. Int. Ed. 2017, 56, 771–775
Self-assembled all-enzyme hydrogels	C <sub>s</sub> -symmetrical 5-nitrononane-2,8-dione	Flow system	75-90%	14000	Angew. Chem. Int. Ed. 2018, 57, 17028–17032
KRED and GDH co-immobilized on aldehyde agarose beads	(S)-2-hydroxy-1-phenylpropan-1-one	Flow system	98%	29.4	Catal. Comm. 2017, 93, 29–32
Mycobacterium smegmatis acetate kinases and the cofactors were fused on DNA frameworks	glycerol	Flow system	83–98%	10839	Nat. Catal. 2019, 2, 1006–1015
NADP(H) recycling in a closed-loop fashion	ethyl 4-chloroacetoacetate	Flow system	93%	2023	Adv. Synth. Catal. 2020, 362, 2894–2901
Enzymes immobilized on magnetic particles	5-nitrononane-2,8-dione	Flow system	95%	4.75	J. Ferment. Technol. 1988, 66, 267-272
Reductase and GDH co-immobilized on magnetic microbeads	pyruvate	Flow system	22%	621	ACS Catal. 2017, 7, 7866–7872
Co-compartmentalization of enzymes and cofactors within Pickering emulsion droplets	2-chloro-3',4'-difluoroacetophenone	Flow system	90-98%	59204	This research

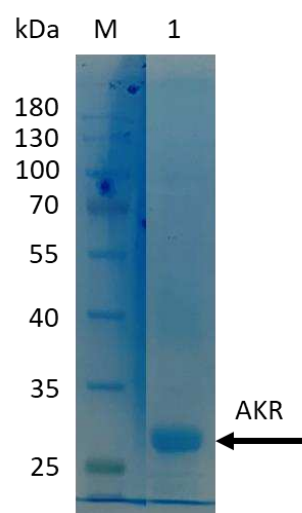


**Fig. S1.** Dodecyl sulfate, sodium salt-polyacrylamide gel electrophoresis (SDS-PAGE) analysis of the AKR solution. Lane M, molecular makers. Lane 1, the AKR solution. The AKR solution was incubated for 10 min at room temperature for UV-Vis determination (595 nm), and the content of protein in enzyme solution was determined to be 35 mg mL<sup>-1</sup>.

Notes: According to the SDS-PAGE analysis results, the molecular weight of the AKR was estimated be 29 kDa.

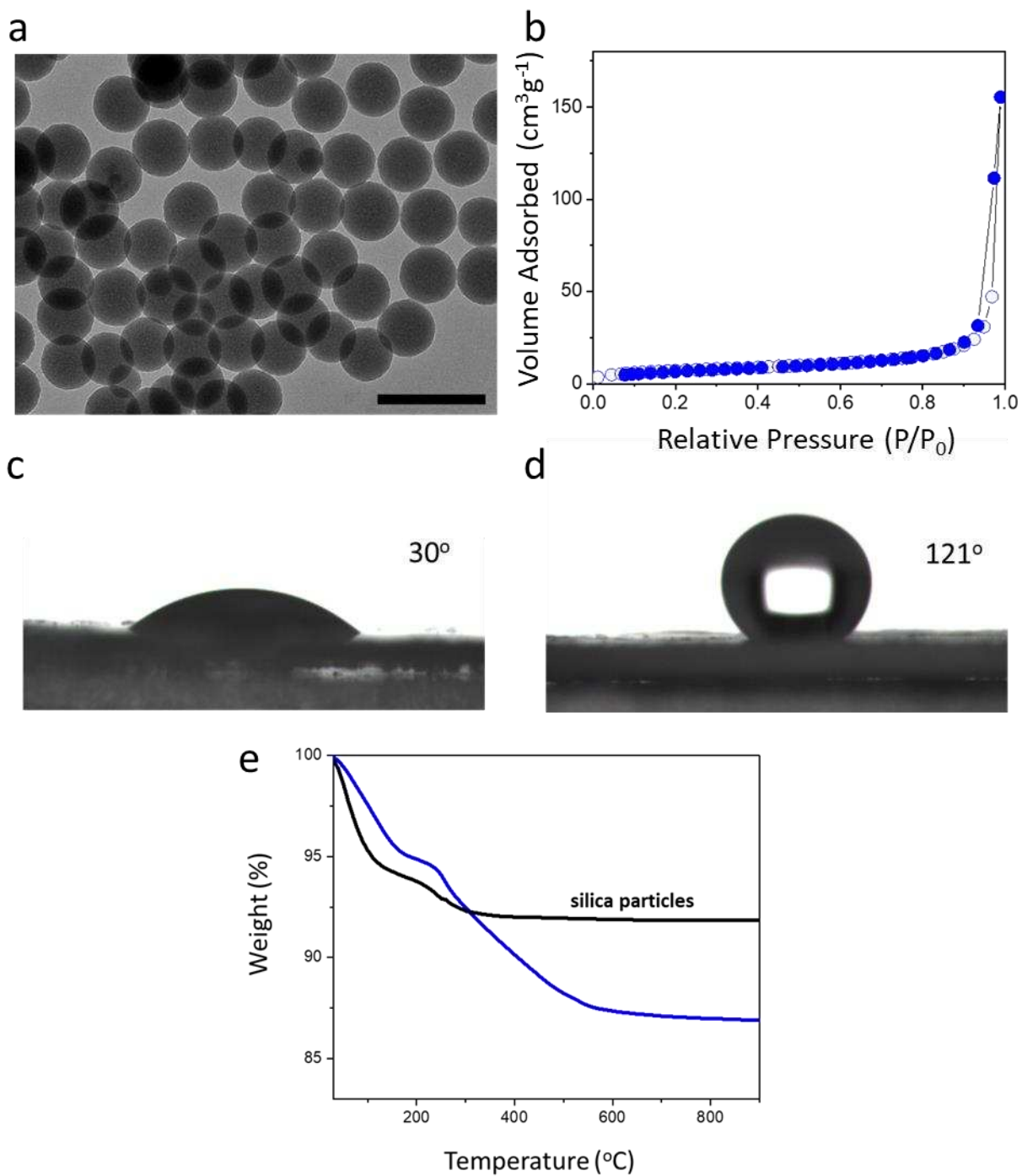


**Fig. S2.** Characterizations of the silica emulsifier. a) TEM image. b) N<sub>2</sub> adsorption-desorption isotherms. c) Appearance of a water droplet in air on a disk of compressed silica particles. d) Appearance of a water droplet in air on a disk of compressed hydrophobically modified silica (emulsifier). e) TG curves of silica particles before and after hydrophobic modification. The TG analyses were performed under air with a heating rate of 10 °C min<sup>-1</sup>. The octyl loading was estimated to be 0.71 mmol g<sup>-1</sup> according to the weight loss in the range of 250-600 °C.

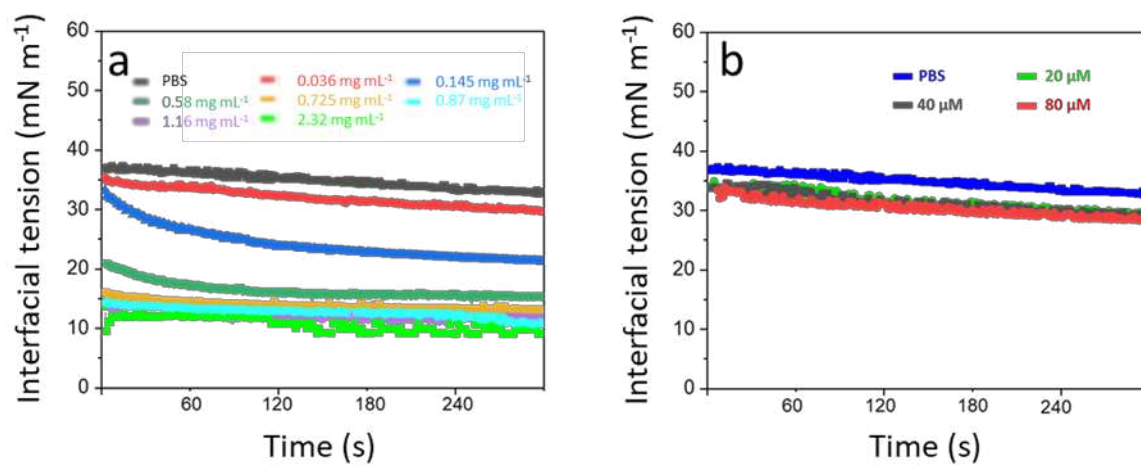


**Fig. S3.** Dynamic interfacial tensions for different water/*n*-heptane biphasic systems. a) Water/*n*-heptane biphasic systems at different concentrations of AKR (with PBS as reference). b) Water/*n*-heptane biphasic systems at different concentrations of NADP<sup>+</sup> (with PBS as reference).

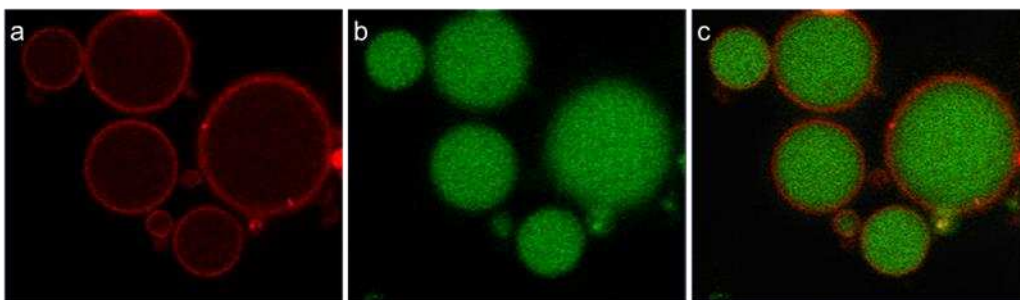


**Figure S4.** Fluorescence microscopy images of Pickering emulsions containing Rhodamine B-labelled AKR or fluorescent NADPH. a) Rhodamine B-labelled AKR. b) Fluorescent NADPH. c) Overlay of (a) and (b).

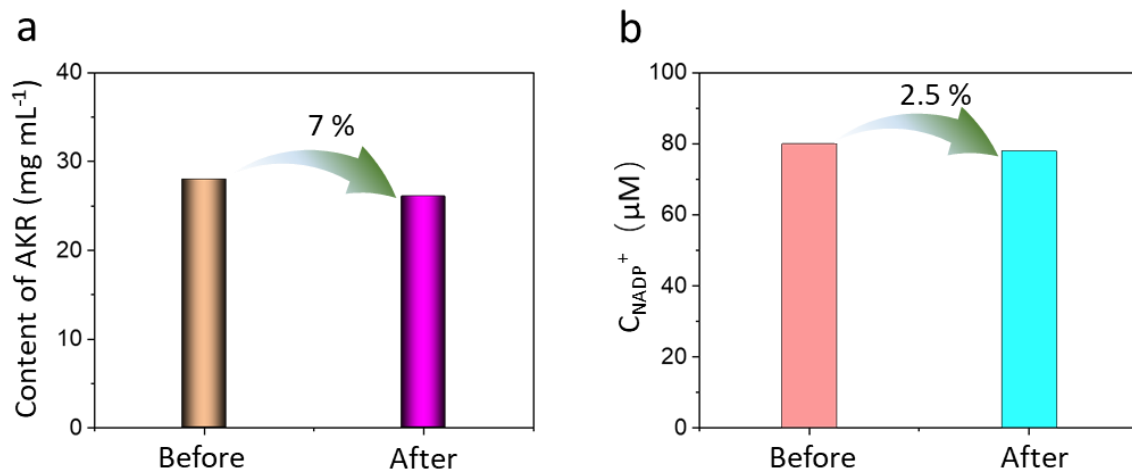


**Fig. S5.** Concentrations of AKR or NADP<sup>+</sup> before and after the continuous flow for 48 h. a) AKR. b) NADP<sup>+</sup>. The Pickering emulsion-based continuous flow system consists of 3.6 mL of PBS, 80 μM NADP<sup>+</sup> and 0.58 mg mL<sup>-1</sup> AKR, 1.8 mL of *n*-heptane, 0.15 g of emulsifier, *n*-heptane as mobile phase, 30 °C, flow rate =5 mL h<sup>-1</sup>. UV-Vis spectrophotometry was used to determine their concentrations. The retention fraction is the ratio of the amount of water-soluble reagent after flow to its amount before flow.

Notes: After 48 h of continuous flow, 93.0% of the initial AKR and 97.5% of the initial NADP<sup>+</sup> were retained within the fixed-bed reactors.

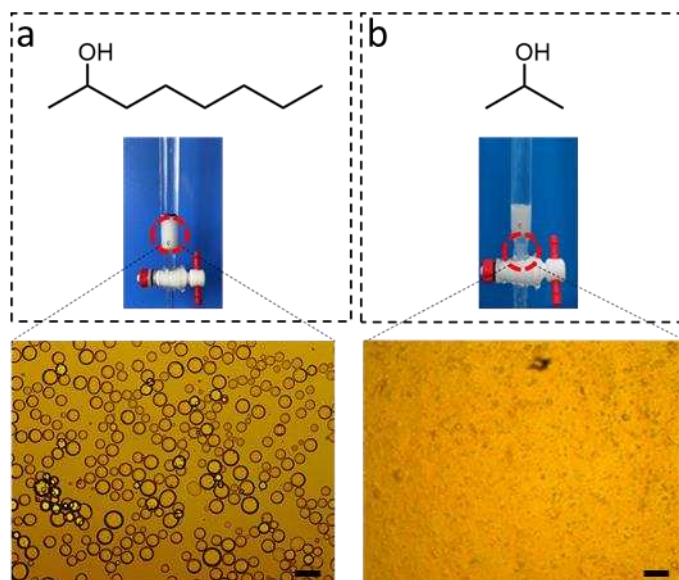


**Fig. S6.** Appearance and optical microscopic images of Pickering emulsions (in a fixed-bed reactor) treated with different mobile phases. a) Treatment with *n*-heptane containing 2-octanol (0.4 M). b) Treatment with *n*-heptane solution containing isopropanol (0.4 M). The Pickering emulsion-based continuous flow system consists of 3.6 mL of PBS, 80  $\mu$ M NADP<sup>+</sup> and 0.58 mg mL<sup>-1</sup> AKR, 1.8 mL of *n*-heptane, 0.15 g of emulsifier, an *n*-heptane solution of 2-octanol or isopropanol as mobile phase, 30 °C, flow rate = 5 mL h<sup>-1</sup>. Scale bar = 100  $\mu$ m.

Notes: The emulsion droplets in the fixed-bed reactor remained intact in terms of morphology after treatment with 2-octanol, whereas the Pickering emulsion was demulsified after treatment with isopropanol.

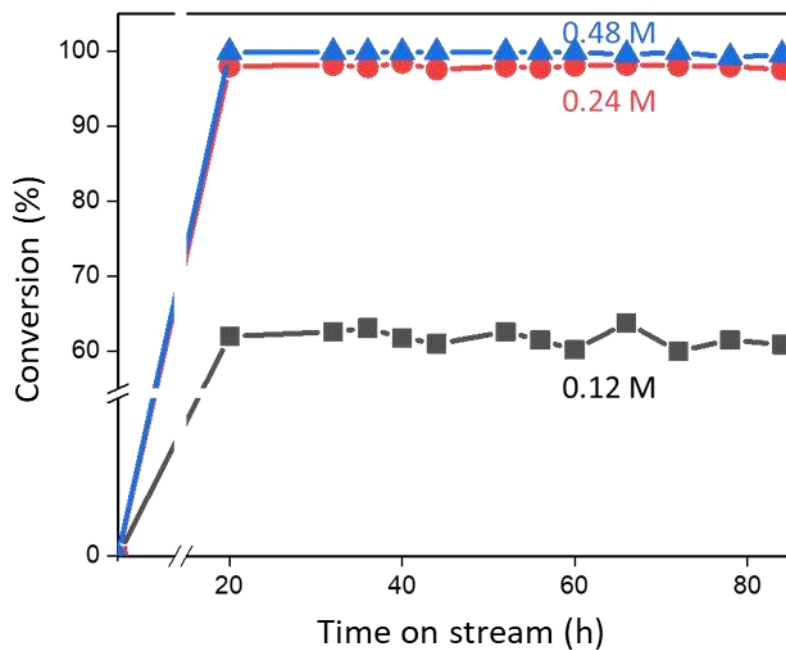


**Fig. S7.** Conversions with time for the enantioselective reduction of 2-chloro-3',4'-difluoroacetophenone in the Pickering emulsion-based continuous flow systems with different concentrations of 2-octanol. The Pickering emulsion-based continuous flow system consists of 3.6 mL of PBS, 80  $\mu$ M NADP<sup>+</sup> and 0.58 mg mL<sup>-1</sup> AKR, 1.8 mL of *n*-heptane, 0.15 g of emulsifier, solution of 2-chloro-3',4'-difluoroacetophenone (0.1 M) and 2-octanol (0.12 M or 0.24 M or 0.48 M) in *n*-heptane as mobile phase, 30 °C, flow rate = 0.5 mL h<sup>-1</sup>.

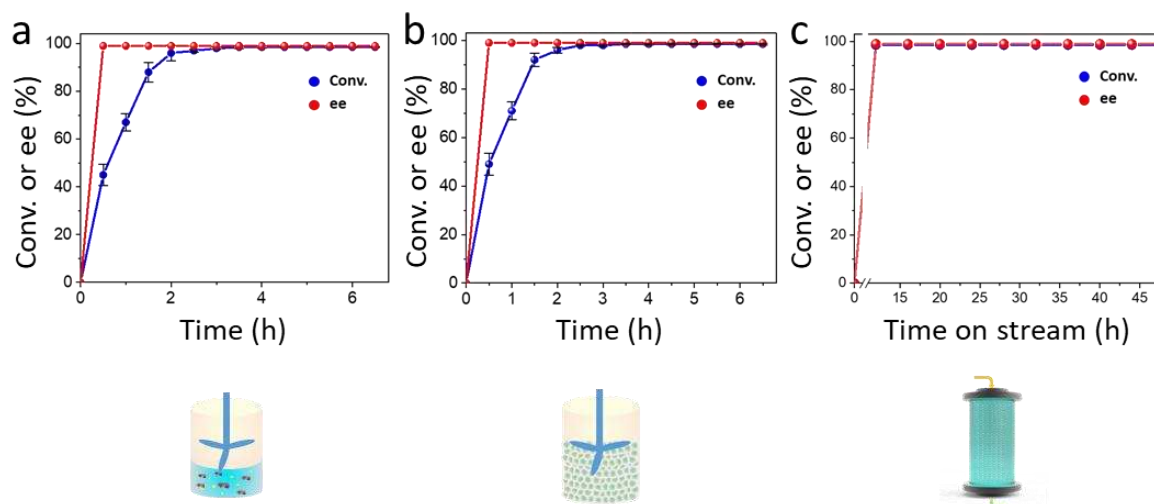


**Fig. S8.** Kinetic profiles for the enantioselective reduction of ethyl 4-chloroacetoacetate in different systems. a) Biphasic system. b) Pickering emulsion-based batch system. c) Pickering emulsion-based continuous flow Pickering emulsion. Reaction conditions for the biphasic system in batch: 0.58 mg mL<sup>-1</sup> AKR, 80 μM NADP<sup>+</sup>, 3.6 mL of PBS, 1.8 mL of *n*-heptane containing ethyl 4-chloroacetoacetate (0.1 M) and 2-octanol (0.24 M), 30 °C, 600 rpm. Reaction conditions for the Pickering emulsion system in batch: Pickering emulsion (formulated with 3.6 mL of PBS, 0.58 mg mL<sup>-1</sup> AKR, 80 μM NADP<sup>+</sup>, 1.8 mL of *n*-heptane, 0.15 g of emulsifier), ethyl 4-chloroacetoacetate (0.1 M) and 2-octanol (0.24 M) in *n*-heptane, 30 °C, 600 rpm. Reaction conditions for the Pickering emulsion-based continuous flow system: Pickering emulsion (formulated with 3.6 mL of PBS, 0.58 mg mL<sup>-1</sup> AKR, 80 μM NADP<sup>+</sup>, 1.8 mL of *n*-heptane, 0.15 g of emulsifier), ethyl 4-chloroacetoacetate (0.1 M) and 2-octanol (0.24 M) in *n*-heptane as mobile phase, 30 °C, flow rate 1.5 mL h<sup>-1</sup>. The specific activities of AKR were calculated according to the conversions within the first 4 h for the batch reactions, whereas the specific activities of AKR were calculated after the conversion leveled off for the continuous flow system.

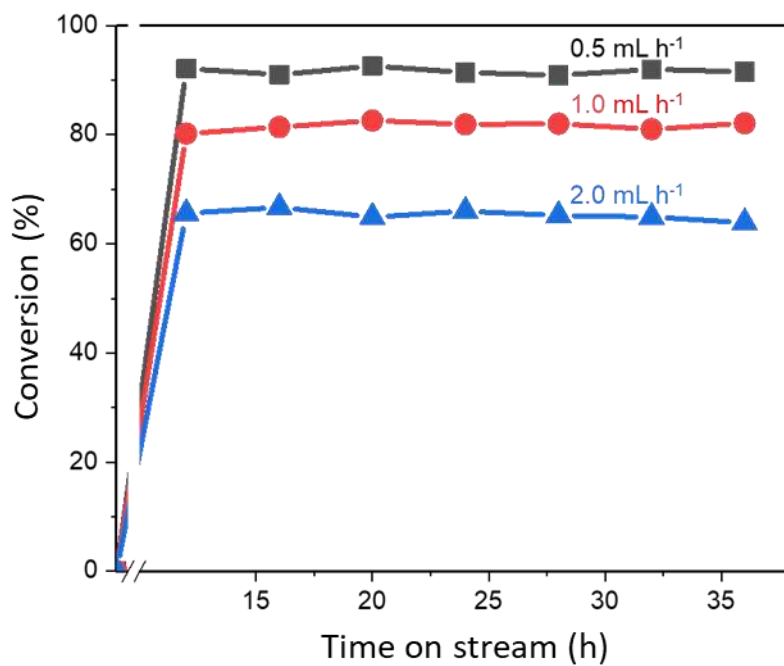


**Fig. S9.** Conversions with time for the enantioselective reduction of 2-chloro-3',4'-difluoroacetophenone in the Pickering emulsion-based continuous flow systems at different flow rates. The Pickering emulsions in the continuous flow systems consist of 3.6 mL of PBS, 80  $\mu$ M NADP<sup>+</sup> and 0.58 mg mL<sup>-1</sup> AKR, 1.8 mL of *n*-heptane, 0.15 g of emulsifier, solution of 2-chloro-3',4'-difluoroacetophenone (0.1 M) and 2-octanol (0.24 M) in *n*-heptane as mobile phase, 30 °C, flow rate = 0.5 mL h<sup>-1</sup> or 1.0 mL h<sup>-1</sup> or 2.0 mL h<sup>-1</sup>.

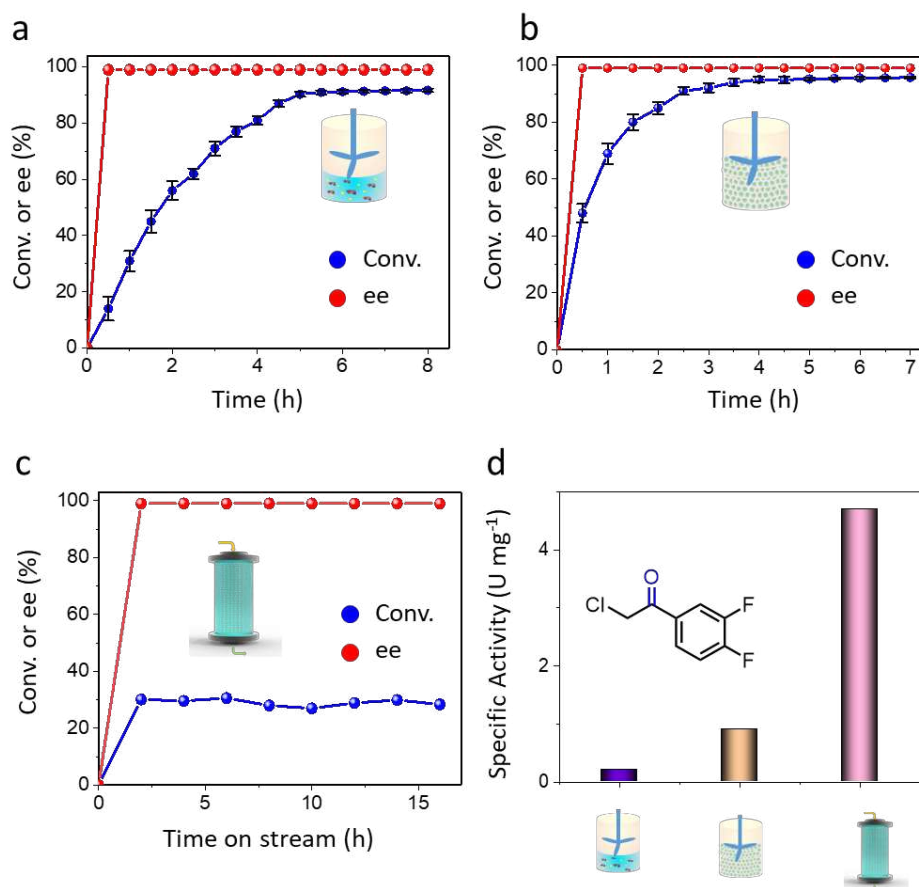


**Figure S10.** Comparison of the specific activity of AKR in batch and continuous flow systems for the enantioselective reduction of 2-chloro-3',4'-difluoroacetophenone. a) Conventional biphasic system in batch. b) Pickering emulsion system in batch. c) Pickering emulsion-based continuous flow system. d) Comparison of the specific activities of AKR in different systems using 2-chloro-3',4'-difluoroacetophenone as substrate. The reaction conditions for the conventional biphasic reaction in batch: 3.6 mL of aqueous AKR (0.58 mg mL<sup>-1</sup>) and NADP<sup>+</sup> (80 μM), 1.8 mL of *n*-heptane containing 2-chloro-3',4'-difluoroacetophenone (0.1 M) and 2-octanol (0.24 M), 30 °C, 600 rpm. The reaction conditions for Pickering emulsion system in batch are the same as those for the conventional biphasic reaction except that 0.15 g emulsifier was added to formulate the Pickering emulsion. Reaction conditions for the Pickering emulsion-based continuous flow system: Pickering emulsion consists of 0.6 mL of *n*-heptane, 1.2 mL of aqueous AKR (0.58 mg mL<sup>-1</sup>) and NADP<sup>+</sup> (80 μM) and 0.05 g of emulsifier, 0.10 M 2-chloro-3',4'-difluoroacetophenone and 0.24 M 2-octanol in *n*-heptane, 30 °C, flow rate = 10.0 mL h<sup>-1</sup>. The specific activity of AKR is calculated based on μmol of substrate converted per milligram of enzyme per min. For the batch reaction, the specific activity was determined in the kinetic region of conversion linearly increasing with time (substrate in much excess). For the continuous flow systems, the specific activity was determined at the high flow rate (but at steady state, substrate in much excess).

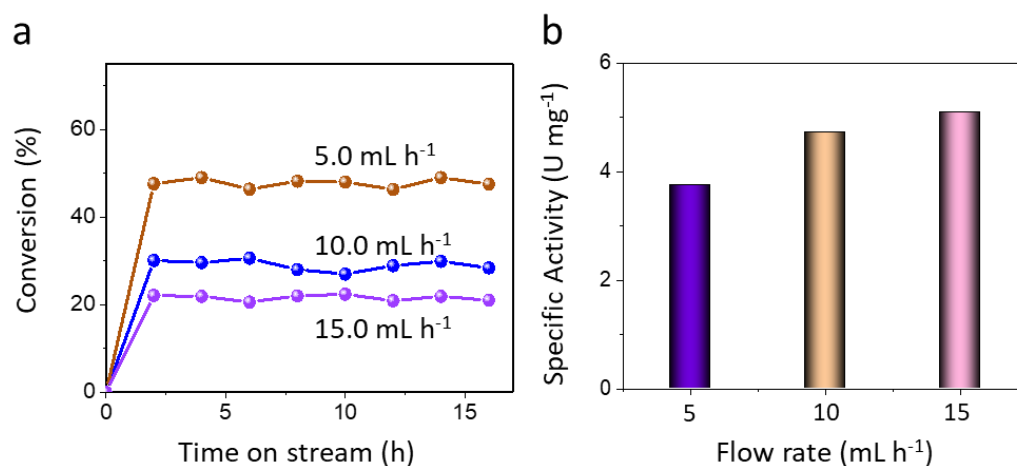


**Figure S11.** Comparison of the specific activity of AKR in the Pickering emulsion-based continuous flow systems at different flow rates. a) Conversions with time for the enantioselective reduction of 2-chloro-3',4'-difluoroacetophenone in the Pickering emulsion-based continuous flow systems at different flow rates. b) Specific activities of AKR in Pickering emulsion-based continuous flow systems with different flow rates. The Pickering emulsions in the continuous flow systems consist of 1.2 mL of PBS, 80  $\mu\text{M}$   $\text{NADP}^+$  and 0.58  $\text{mg mL}^{-1}$  AKR, 0.6 mL of *n*-heptane, 0.05 g of emulsifier, solution of 2-chloro-3',4'-difluoroacetophenone (0.1 M) and 2-octanol (0.24 M) in *n*-heptane as mobile phase, 30 °C, flow rate = 5.0  $\text{mL h}^{-1}$  or 10.0  $\text{mL h}^{-1}$  or 15.0  $\text{mL h}^{-1}$ . The specific activity of AKR is calculated based on  $\mu\text{mol}$  of substrate converted per milligram of enzyme per min. For the batch reaction, the specific activity was determined in the kinetic region of conversion linearly increasing with time (substrate in much excess). For the continuous flow system, the specific activity was determined at the high flow rate (but at steady state, substrate in much excess).

Notes: When the flow rate was increased from 5.0 to 10.0 and further to 15.0  $\text{mL h}^{-1}$ , the specific activity of AKR increased from 3.79 (48%) to 4.72 (30%) and then to 5.10 (22%)  $\text{U mg}^{-1}$ . This results point to a flow effects that continuous flow system is favorable to improve the specific activity.

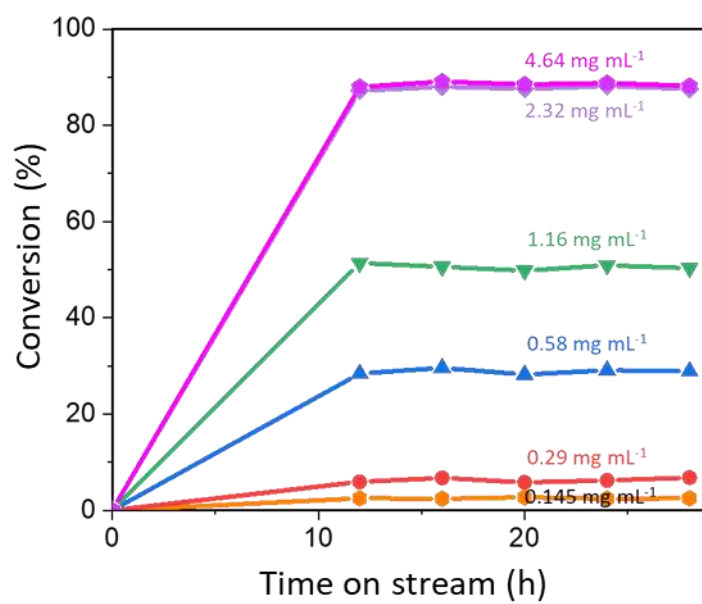


**Fig. S12.** Conversions with time for the enantioselective reduction of 2-chloro-3',4'-difluoroacetophenone in Pickering emulsion-based continuous flow systems with different concentrations of AKR. The Pickering emulsions in the continuous flow systems consist of 3.6 mL of PBS, 80  $\mu$ M NADP<sup>+</sup> and different concentrations of AKR, 1.8 mL of *n*-heptane, 0.15 g of emulsifier, solution of 2-chloro-3',4'-difluoroacetophenone (0.1 M) and 2-octanol (0.24 M) in *n*-heptane as mobile phase, 30 °C, flow rate =1.5 mL h<sup>-1</sup>.

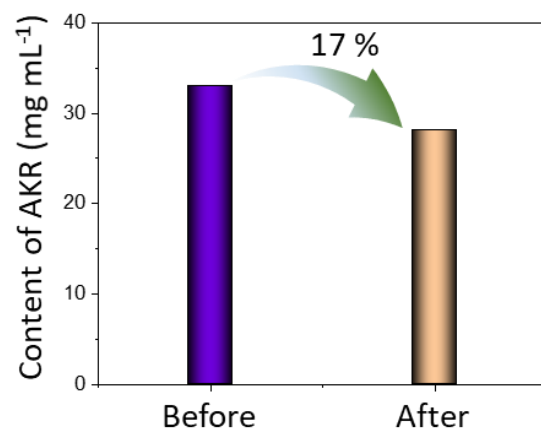


**Fig. S13.** Concentrations of AKR in the PBS solution before and after the addition of emulsifier. The AKR concentrations were determined by UV-Vis, and AKR solution was stirred with emulsifier for 12 h for measurements. The retention fraction is the ratio of the amount of water-soluble reagent after stirring to its amount before stirring.

Notes: According to the UV-Vis results, it was estimated that 17.0% of the initial AKR was adsorbed at the emulsifier surface.

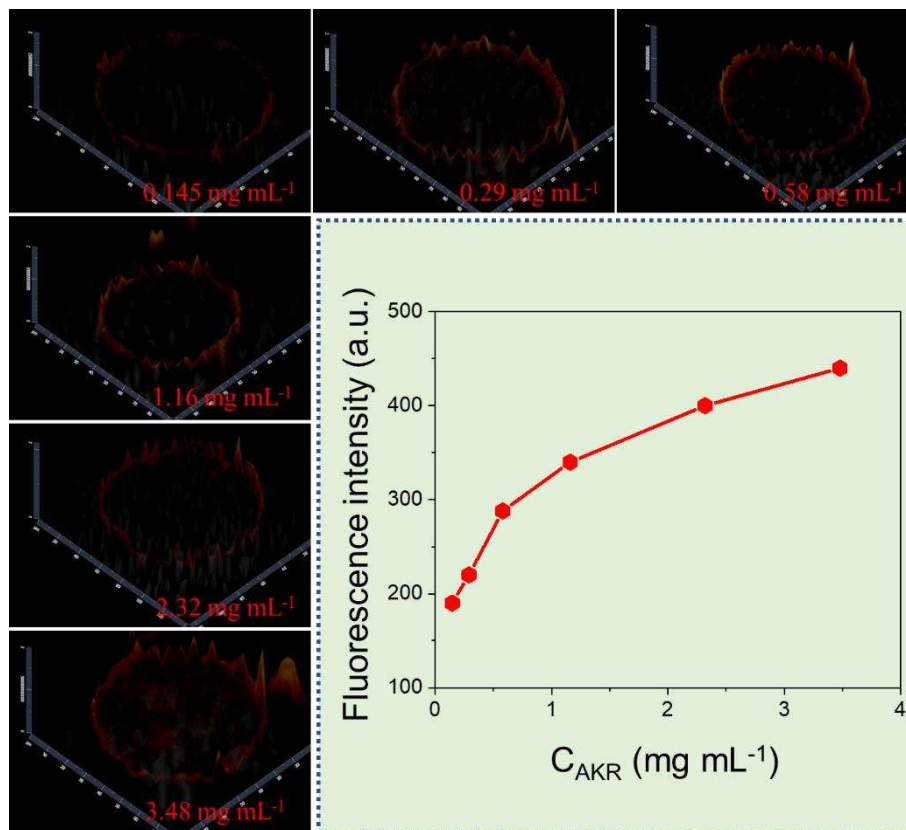


**Figure S14.** 2.5D confocal fluorescence microscopy images showing the distribution of Rhodamine B-labelled AKR at the droplet interface at different AKR concentrations. The Pickering emulsions consist of 3.6 mL of PBS, 80  $\mu$ M NAD<sup>+</sup> and different concentrations of AKR, 1.8 mL of *n*-heptane, 0.15 g of emulsifier. The AKR is labelled with Rhodamine B and fluorescence intensity of the droplet at different AKR concentrations was observed by fluorescence microscopy.

Notes: With the AKR concentration increasing, the fluorescent intensity at the droplet interfaces gradually increased, while the interior of droplet has almost no fluorescent signals. These observations indicate that most of enzymes tend to aggregate at the droplet interfaces despite the presence of the silica particles.

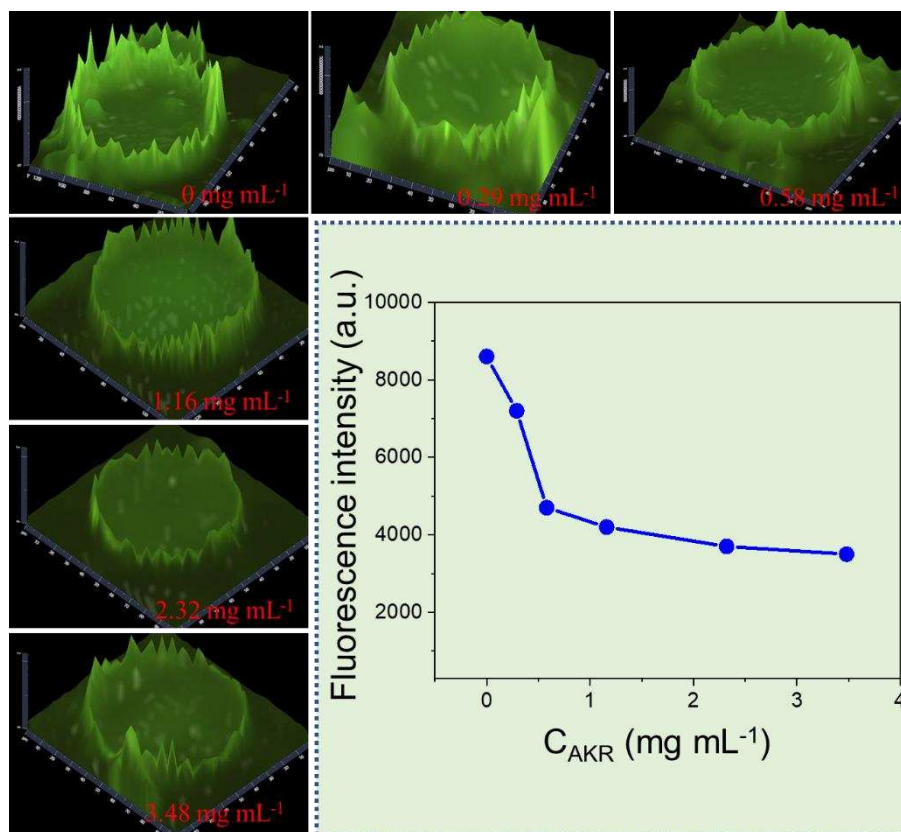


**Figure S15.** 2.5D confocal fluorescence microscopy images showing the distribution of FITC-labelled solid emulsifier at the droplet interface at different AKR concentrations. The Pickering emulsions consist of 3.6 mL of PBS, 80  $\mu$ M NADP<sup>+</sup> and different concentrations of AKR, 1.8 mL of *n*-heptane, 0.15 g of emulsifier. The emulsifier is labelled with FITC and the fluorescence intensity of droplet at different AKR concentrations was observed by fluorescence microscopy.

Notes: With the AKR concentration increasing, the fluorescent intensity at the interfaces first decreased, and then gradually leveled off when the enzyme concentration is beyond 0.58 mg mL<sup>-1</sup>. This suggests that the amount of silica emulsifier at the interfaces gradually decreased as the enzyme concentration increased, and above a threshold enzyme concentration the amount of silica emulsifier at the interfaces no longer changed.

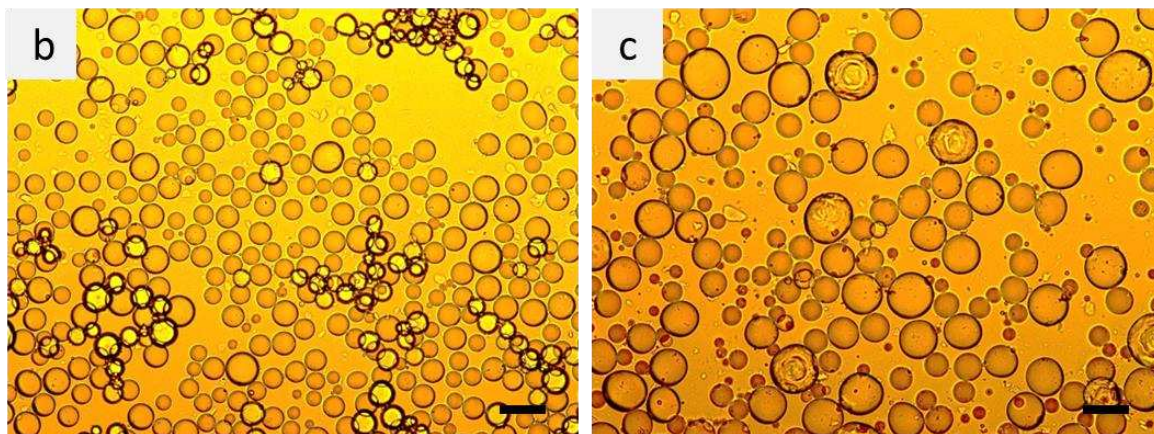
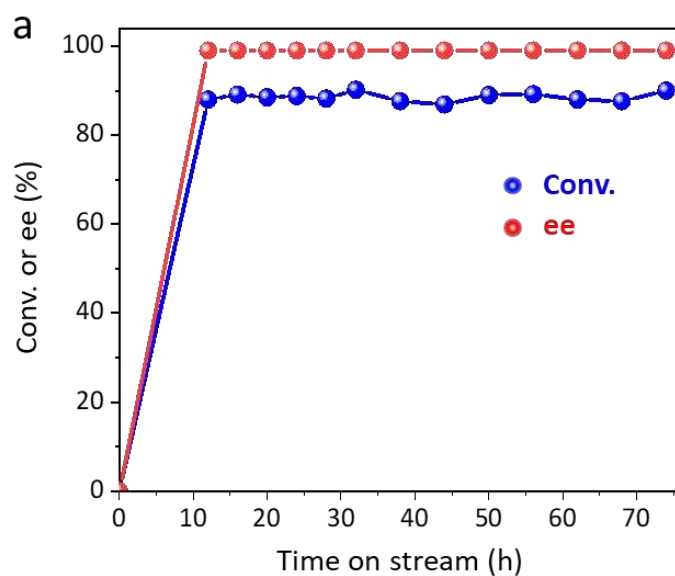


**Figure 16.** The results for the enantioselective reduction of 2-chloro-3',4'-difluoroacetophenone in Pickering emulsion-based continuous flow system at a high concentration of AKR and optical micrographs of the Pickering emulsions before and after 75 h of continuous flow reaction. a) Conversions with time for the enantioselective reduction of 2-chloro-3',4'-difluoroacetophenone in Pickering emulsion-based continuous flow system at a high concentration of AKR. b) Optical micrographs of the Pickering emulsions before continuous flow reaction. c) Optical micrographs of the Pickering emulsions after 75 h of continuous flow reaction. Scale bar = 50  $\mu\text{m}$ . The Pickering emulsions in the continuous flow system consists of 3.6 mL of PBS, 80  $\mu\text{M}$  NADP<sup>+</sup> and 4.64  $\text{mg mL}^{-1}$  AKR, 1.8 mL of *n*-heptane, 0.15 g of emulsifier, solution of 2-chloro-3',4'-difluoroacetophenone (0.1 M) and 2-octanol (0.24 M) in *n*-heptane as mobile phase, 30 °C, flow rate =0.5  $\text{mL h}^{-1}$ .

Notes: In order to test the long-term stability of the Pickering emulsions in the presence of enzyme, a fixed-bed reactor packed with a Pickering emulsion containing a high concentration of enzyme (4.64  $\text{mg mL}^{-1}$ ) was investigated. As shown in Figure S16a, the conversions were maintained above 90% during 75 h of continuous reaction monitored. The droplets were virtually unchanged in respect to morphology and sizes when compared with the droplets before reaction (Figures 16b and 16c). These results show that even in the presence of highly concentrated enzyme our Pickering emulsion droplets-based continuous flow system still has a good operational stability.

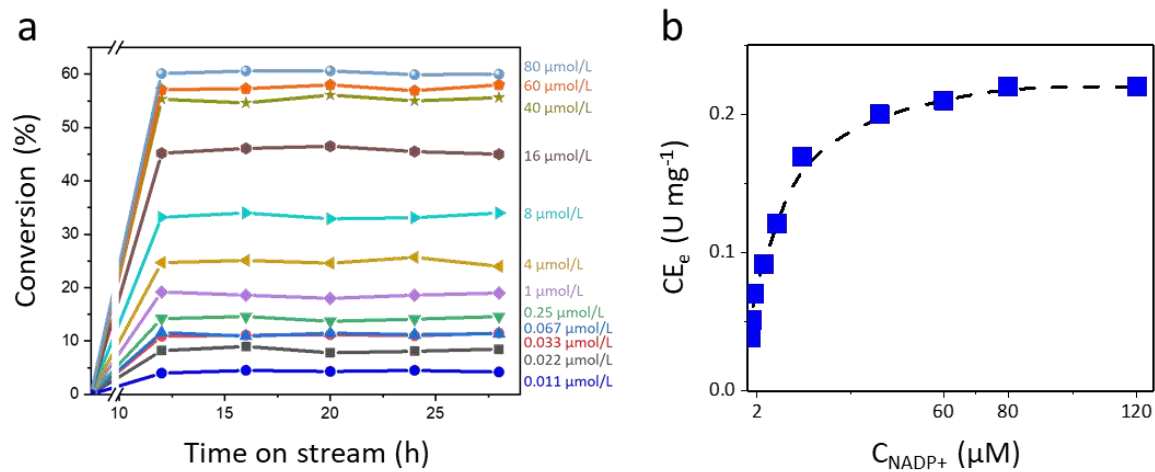


**Fig. S17.** Pickering emulsion-based continuous flow systems with different concentrations of NADP<sup>+</sup>. a) Conversions with time for the enantioselective reduction of 2-chloro-3',4'-difluoroacetophenone in Pickering emulsion-based continuous flow systems with different concentrations of NADP<sup>+</sup>. b) Catalytic efficiency of AKR (CE<sub>e</sub>) as a function of NADP<sup>+</sup> concentration. The Pickering emulsions in continuous flow systems consist of 3.6 mL of PBS, different concentrations of NADP<sup>+</sup> and 0.58 mg mL<sup>-1</sup> AKR, 1.8 mL of *n*-heptane, 0.15 g of emulsifier, solution of 2-chloro-3',4'-difluoroacetophenone (0.1 M) and 2-octanol (0.24 M) in *n*-heptane as mobile phase, 30 °C, flow rate = 1.5 mL h<sup>-1</sup>.

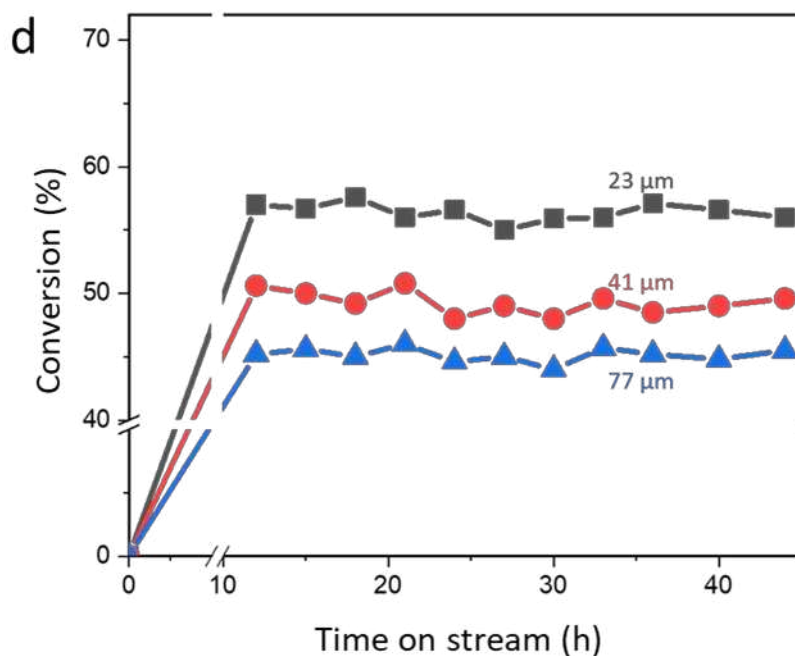
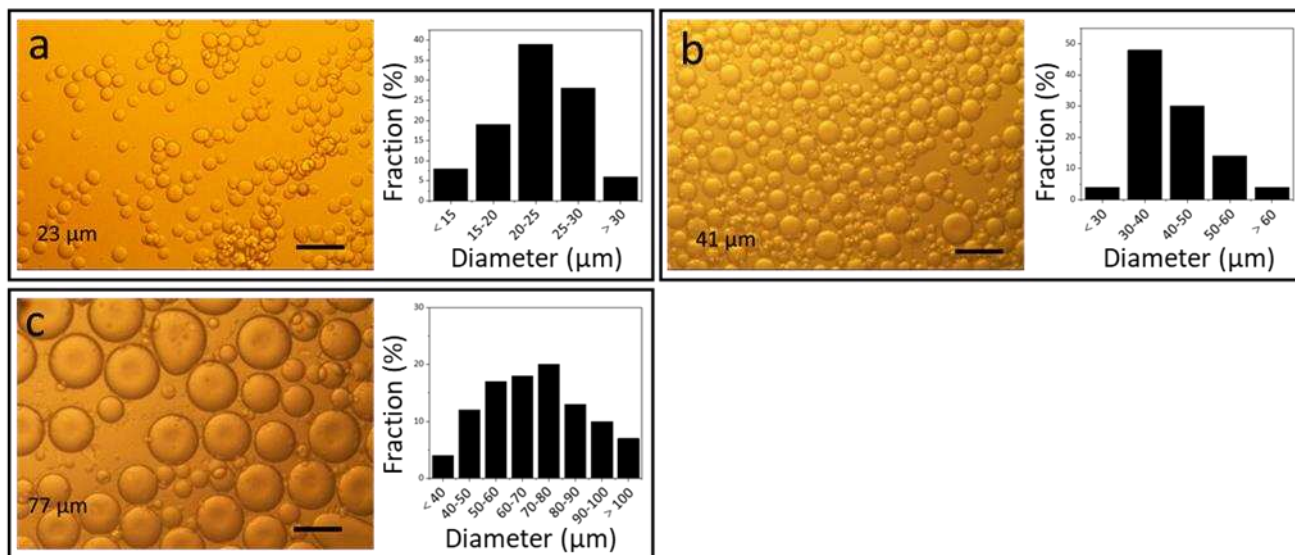


**Fig. S18.** Optical micrographs of Pickering emulsions with different droplet sizes and the results for the enantioselective reduction of 2-chloro-3',4'-difluoroacetophenone in Pickering emulsion-based continuous flow systems with different droplet sizes. a) 23  $\mu\text{m}$ . b) 41  $\mu\text{m}$ . c) 77  $\mu\text{m}$ . d) Conversions as a function of time for Pickering emulsion droplets with different sizes. Scale bar = 100  $\mu\text{m}$ . The Pickering emulsion-based continuous flow systems consist of 3.6 mL of PBS, 80  $\mu\text{M}$  NADP<sup>+</sup> and 0.58 mg mL<sup>-1</sup> AKR, 1.8 mL of *n*-heptane, 0.15 g of emulsifier, solution of 2-chloro-3',4'-difluoroacetophenone (0.1 M) and 2-octanol (0.24 M) in *n*-heptane as mobile phase, 30 °C, flow rate = 1.5 mL h<sup>-1</sup>. The preparation of Pickering emulsions with different droplet sizes is provided in Experimental Section in the Supporting Information.

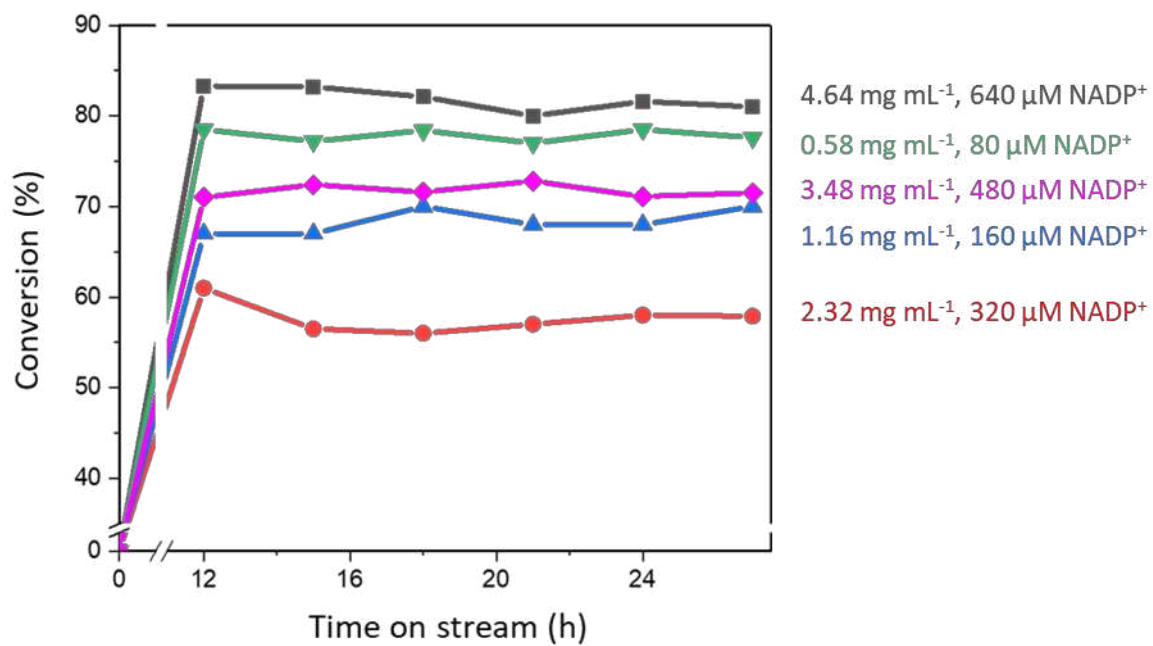


**Fig. S19.** Conversions with time for the enantioselective reduction of 2-chloro-3',4'-difluoroacetophenone in Pickering emulsion-based continuous flow systems with different AKR or NADP<sup>+</sup> concentrations (the amounts of AKR and NADP<sup>+</sup> are fixed and their molar ratio is fixed at about 1:4). The Pickering emulsions in the continuous flow systems consist of different amounts of PBS, different concentrations of NADP<sup>+</sup> and different concentrations of AKR, a given amount of emulsifier, solution of 2-chloro-3',4'-difluoroacetophenone (0.1 M) and 2-octanol (0.24 M) in *n*-heptane as mobile phase, 30 °C, flow rate = 1.5 mL h<sup>-1</sup>.

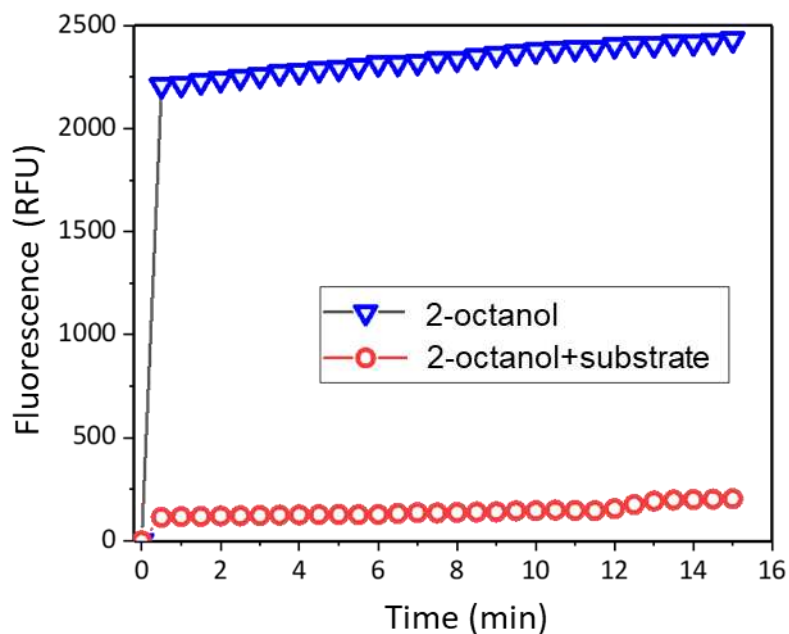


**Fig. S20.** Fluorescence intensity of NADPH as a function of time for the case with or without the addition of substrate. The fluorescence was measured at a wavelength of 460 nm.

Notes: According to the reaction mechanism (Figure 1A), when 2-octanol was added into the Pickering emulsion system,  $\text{NADP}^+$  was converted back to NADPH through AKR-catalyzed oxidation of 2-octanol to 2-octanone. If the reaction system is absent of the substrate (for example 2-chloro-3',4'-difluoroacetophenone), NADPH was not consumed. Because NADPH itself can generate fluorescent signals at a wavelength of 460 nm whereas  $\text{NADP}^+$  doesn't. The change of NADPH content in water can be determined according to its fluorescence intensity. To confirm that  $\text{NADP}^+$  can be regenerated within the Pickering emulsion droplets, we examined two systems for comparison. In the first Pickering emulsion reaction system, 2-octanol and AKR were added but no any substrates were added. It was found that the NADPH concentration did not change with time. However, in the second Pickering emulsion reaction system, 2-chloro-3',4'-difluoroacetophenone, 2-octanol and AKR were added, and it was found the NADPH concentration rapidly decreased to a very low level, indicating all NADPH molecules were consumed, converting to  $\text{NADP}^+$ .

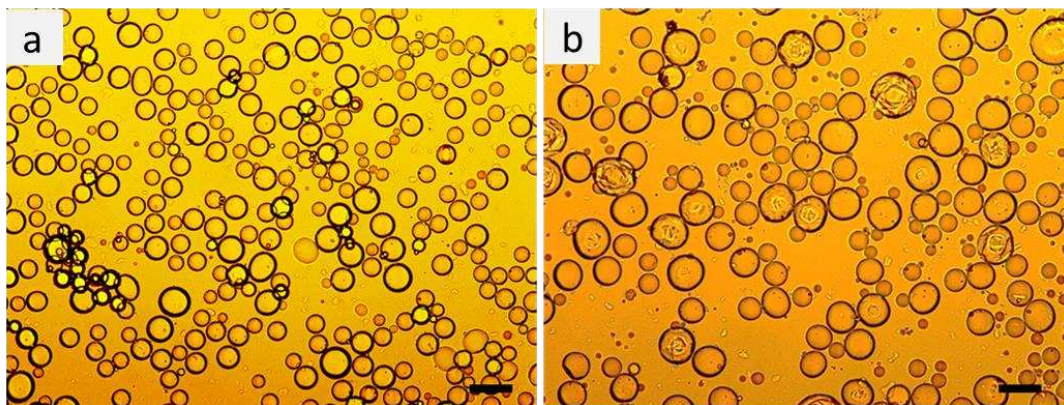


**Fig. S21.** Optical micrographs of the Pickering emulsions before and after 300 h of continuous flow reaction. a) Before reaction. b) After reaction. Scale bar = 50  $\mu\text{m}$ .

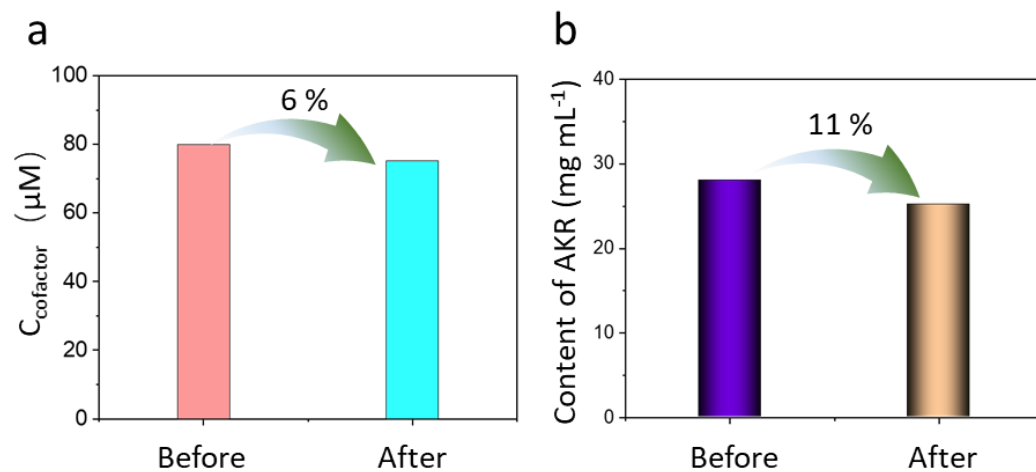


**Fig. S22.** Concentrations of NADP<sup>+</sup> or AKR before and after 300 h of the continuous flow reaction. a) NADP<sup>+</sup>. b) AKR. The AKR and NADP<sup>+</sup> contents in aqueous phase were determined by UV-Vis. Other reaction conditions are the same as in Figure 4. The retention fraction is defined as the ratio of the amount of AKR or NADP<sup>+</sup> after the continuous flow reactions to its amount before the continuous flow reaction.

Notes: After 300 h of continuous flow, 89.0% of the initial AKR and 94.0% of the initial NADP<sup>+</sup> were retained within the fixed-bed reactor. The determination methods are provided in Experimental Section in the Supporting Information.

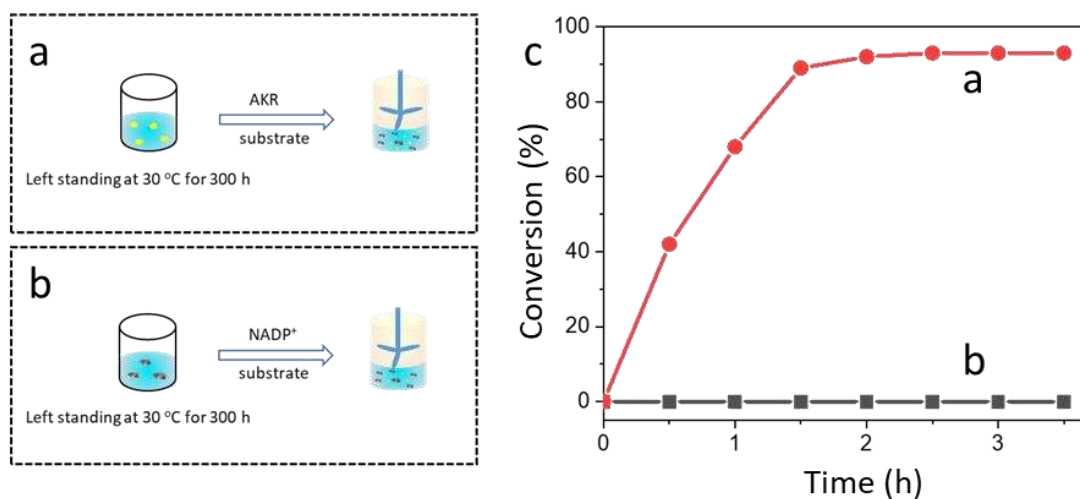


**Fig. S23.** Scheme illustrations and kinetic plots for batch reactions after standing NADP<sup>+</sup> or AKR at 30 °C for 300 h. Reaction conditions: a) Scheme illustration for the NADP<sup>+</sup> solution (80 μM) was left standing for 300 h, and then AKR was added to conduct the reaction. b) Scheme illustration for the AKR solution (0.58 mg mL<sup>-1</sup>) was left standing for 300 h, and then cofactor was added to conduct the reaction. c) Kinetic plots for batch reactions after standing NADP<sup>+</sup> or AKR at 30 °C for 300 h.

Notes: After the NADP<sup>+</sup> solution was left standing for 300 h, a 92% conversion was obtained (Graph a). However, after an aqueous solution of AKR was left standing for 300 h, cofactors, substrate and co-substrate were added to the system, but almost no substrate was converted (Graph b). These results point to the fact that the decrease in catalysis efficiency is caused by deactivation of AKR instead of NADP<sup>+</sup>.

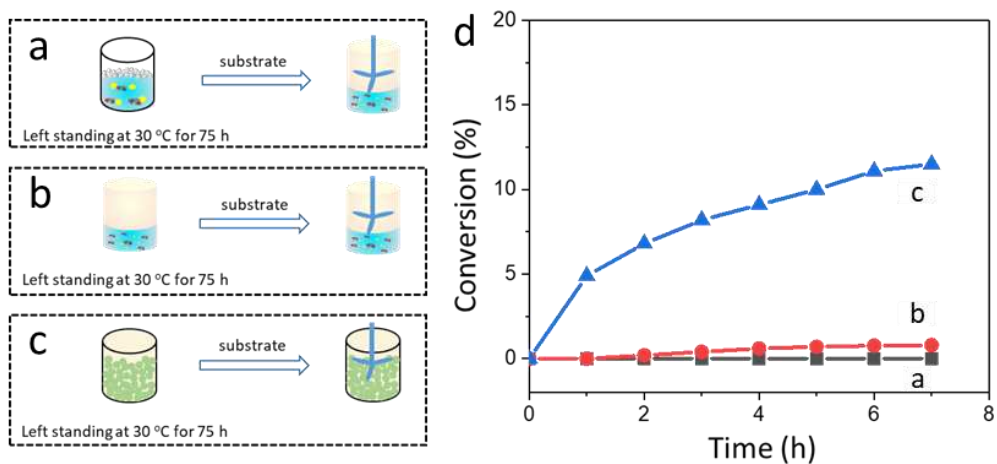


**Fig. S24.** Scheme illustrations and kinetic plots of different experiments reveal the reason for enzyme deactivation. a) Scheme illustration for the aqueous solution containing AKR, NADP<sup>+</sup> and emulsifier was left standing at 30 °C for 75 h, substrate and co-substrate were added. b) Scheme illustration for the heptane/water biphasic system containing AKR and NADP<sup>+</sup> was left standing at 30 °C, substrate and co-substrate were added. c) Scheme illustration for the Pickering emulsion system containing AKR and NADP<sup>+</sup> was left standing at 30 °C, substrate and co-substrate were added. d) Kinetic plots for batch reactions of different experiments.

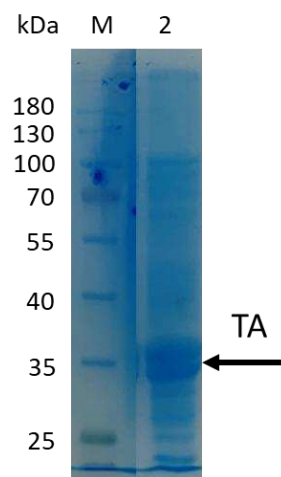


**Fig. S25.** SDS-PAGE analysis of the TA solution. Lane M, molecular makers. Lane 2, the TA solution. The TA solution was incubated for 10 min at room temperature for UV-Vis determination (595 nm), and the content of protein in the enzyme solution was determined to be 48 mg mL<sup>-1</sup>.

Notes: According to the SDS-PAGE analysis results, the molecular weight of the TA was estimated to be 33 kDa.

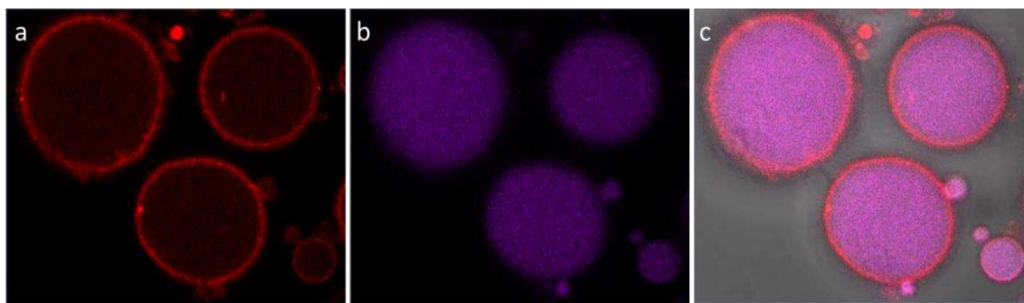


**Figure S26.** Fluorescence microscopy images of Pickering emulsions containing Rhodamine B-labelled TA or fluorescent PLP. a) Rhodamine B-labelled TA. b) Fluorescent PLP. c) Overlay of (a) and (b).

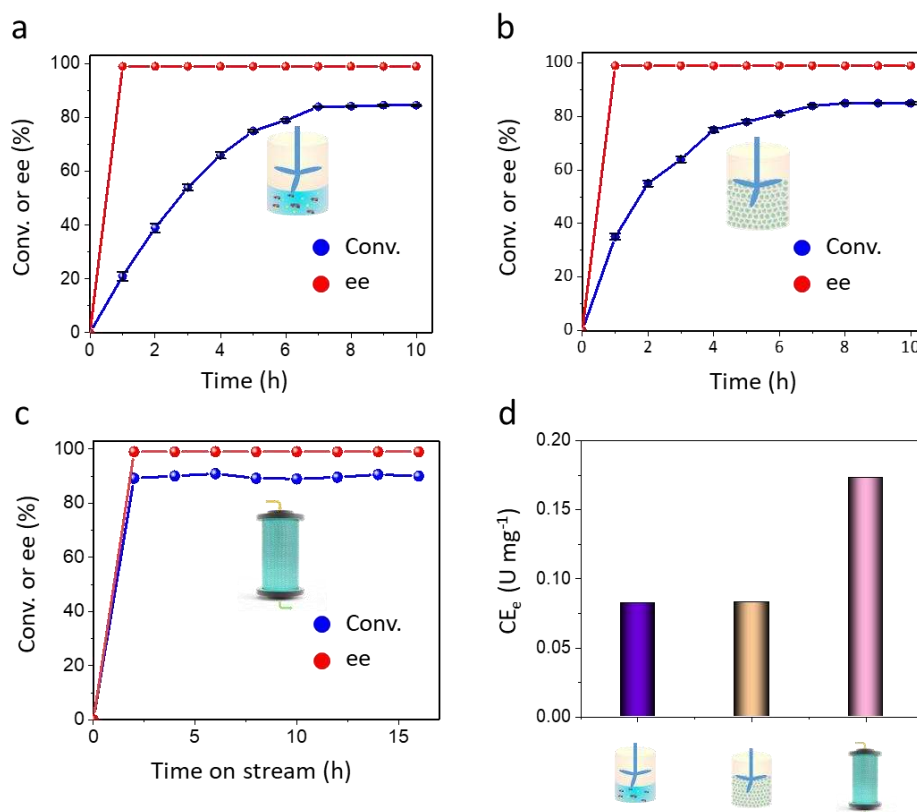


**Figure S27.** Comparison of the catalytic efficiency of TA in batch and continuous flow systems for the enantioselective transamination of 4'-nitroacetophenone. a) Conventional biphasic system in batch. b) Pickering emulsion system in batch. c) Pickering emulsion-based continuous flow system. d) Comparison of the catalytic efficiencies of TA in different systems using 4'-nitroacetophenone as substrate. The reaction conditions for the conventional biphasic reaction in batch: 6.0 mL of aqueous TA (0.36 mg mL<sup>-1</sup>) and PLP (0.75 mM), 2.0 mL of toluene containing 4'-nitroacetophenone (0.05 M) and phenylethylamine (0.20 M), 45 °C, 600 rpm. The reaction conditions for Pickering emulsion system in batch are the same as those for the conventional biphasic reaction except that 0.18 g emulsifier was added to formulate the Pickering emulsion. Reaction conditions for the Pickering emulsion-based continuous flow system: Pickering emulsion consists of 3.0 mL of toluene, 6.0 mL of aqueous TA (0.36 mg mL<sup>-1</sup>) and PLP (0.75 mM) and 0.18 g of emulsifier, 0.05 M 4'-nitroacetophenone and 0.20 M phenylethylamine in toluene, 45 °C, flow rate = 0.5 mL h<sup>-1</sup>. The catalytic efficiency of enzyme (CE<sub>e</sub>, U mg<sup>-1</sup>) is defined as μmol of substrate converted per milligram of enzyme per min. For batch reactions, CE<sub>e</sub> is estimated when the substrate approaches a nearly full conversion (within the first 8 h in this work); for continuous flow reactions, CE<sub>e</sub> is calculated at steady state (μmol of substrate converted within 60 min per milligram of enzyme per 60 min). The catalytic efficiencies of AKR were calculated according to the conversions within the first 8 h for the batch reactions, and after the conversion leveled off for the continuous flow reactions.

Mass spectrometry data for various compounds encountered in this study

